ANL/ET/CP-93514

EFFECT OF Fe- AND Si-INDUCED FLAWS ON FRACTURE OF Si_3N_4*

CONF-971012--

J. P. Singh

Energy Technology Division
Argonne National Laboratory
9700 South Cass Avenue
Argonne, Illinois 60439 USA

October 1997

Invited paper to be presented at 6th International Symposium on Ceramic Materials & Components for Engines, Arita, Japan, October 19-24, 1997.

*Research sponsored by Office of Fossil Energy, U.S. Department of Energy, Advanced Research and Technology Development Fossil Energy Materials Program DOE/FE AA 15 10 10 0, Work Breakdown Structural Element ANL 1, under Contract W-31-109-Eng-38.

DISCLAIMER

EFFECT OF Fe- AND Si-INDUCED FLAWS ON FRACTURE OF Si_3N_4

J. P. Singh

Energy Technology Division, Argonne National Laboratory
9700 South Cass Avenue, Argonne, Illinois 60439 USA

ABSTRACT

Fracture studies were performed to detect and assess the effect of flaws on the fracture behavior of hot-pressed Si_3N_4 with Fe or Si inclusions. The addition of 5 and 0.5 wt.% Fe inclusions of 88-250 μm size reduced the strength of Si_3N_4 specimens by ≈40 and 15%, respectively. Similarly, addition of 1 and 0.5 wt.% Si inclusions of <149 μm size reduced the strength of Si_3N_4 specimens by ≈50 and 39%, respectively. Fractography indicated that failure occurred primarily from internal flaws which included Fe- and Si-rich inclusions and/or regions of Si_3N_4 matrix that were degraded as a result of reaction between Si_3N_4 and molten Fe or Si. For inclusion-induced internal flaws, the critical flaw sizes calculated by fracture mechanics were always larger than the fractographically measured flaw sizes. This observation suggested local degradation in fracture toughness of the Si_3N_4 matrix. A ratio, K, of ≈3.5-4.2 appeared to exist between the calculated and measured values of the critical internal flaw sizes of specimens that contained Fe inclusions. A similar ratio of 1.7-3.1 was observed for specimens that containd Si inclusions. The ratio K has important implications for strength predictions that are based on observed flaw size.

INTRODUCTION

Si_3N_4 has been recognized as a candidate for structural applications in advanced heat engines (gas turbine, diesel)[1,2] and many other devices[3] because of its potentially excellent mechanical integrity and resistance to oxidation and corrosion at high temperatures. However, it has been observed that the mechanical behavior of Si_3N_4 and other polycrystalline ceramics, in general, is controlled by the size, number, and distribution of extrinsic and intrinsic flaws,[4-6] such as machining flaws, pores, agglomerates, inclusions, and other microstructural irregularities. These flaws are, in many cases, introduced during various stages of fabrication, machining and service. The characteristics and density of these flaws depend on the fabrication technique (green pressing, slip casting, sintering, hot pressing, etc.). Evaluation of the effect of these flaws on fracture properties of specimens made by differing techniques will provide information for the control of fabrication and machining procedures.

This paper presents the results of a study that evaluated the effect of well-characterized Fe- and Si-induced flaws on fracture behavior of hot-pressed Si_3N_4. Because inclusions rich in Fe and Si have been observed to cause substantial degradation of the strength of Si_3N_4, this study was conducted on Si_3N_4-Fe and Si_3N_4-Si systems.

EXPERIMENTAL PROCEDURES

Specimen Preparation

Dense specimens of Si_3N_4 were hot pressed from two commercial powders, designated Si_3N_4-A and Si_3N_4-B . Each powder was wet milled in a solution of 30% isopropyl alcohol and 70% water for 16 h; Al_2O_3 balls served as the grinding medium. Si_3N_4 powders were mixed with 6 wt.% Y_2O_3 as a densification aid. The mixtures were again wet milled for 16 h and then spray dried. The spray-dried powder mixtures were hot pressed in a boron-coated graphite die at 1750°C and 22 MPa for 2 h in a high-purity N_2 atmosphere. Some Si_3N_4 specimens were seeded with Fe or Si inclusions by hot pressing a powder mixture of Si_3N_4-A with 6 wt.% Y_2O_3 and 0.5 and 5 wt.% of 88-250 μm Fe inclusions or 0.5 and 1 wt.% of <149-μm Si powder at 1725°C for 2 h with the die, pressure, and gas atmosphere described above.

After the density of the hot-pressed disks was measured by the buoyancy method, the disks were ground to a standard surface finish on a 45-32-μm diamond wheel. Modulus of rupture (MOR) bars (≈3.8 x 0.4 x 0.3 cm) were subsequently machined from the disks; the cut faces of the bars were ground on a 32-μm diamond wheel, and the edges were bevelled. The bars were used to measure mechanical properties and to conduct fractographic studies.

Mechanical Property Measurement and Fractography

To measure flexural strength, the MOR bars were fractured in a four-point-bending mode with a support span of 3.18 cm, loading span of 0.953 cm, and a crosshead speed of 0.13 cm/min. The fracture surfaces of the broken bars were examined by optical and electron microscopy to establish fracture modes and to locate failure-initiating critical flaws. Low-magnification, optical microscopy was used to find the general location of the critical flaws by

identifying fracture markings such as fracture mirrors and river patterns.[7-8] Subsequently, scanning electron microscopy (SEM) was used to find the exact location and identify details of the critical flaws. Fracture toughness (K_{IC}) was measured by indentation techniques[9] and elastic modulus (E) was evaluated by the pulse-echo technique.[10]

RESULTS AND DISCUSSIONS

Mechanical Properties and Fractography

Although this study focused primarily on specimens of Si_3N_4 that were seeded with Fe or Si inclusions, limited results for unseeded Si_3N_4-A and Si_3N_4-B specimens will also be presented to establish a data base for the purpose of comparison.

The densities of hot-pressed Si_3N_4-A and Si_3N_4-B specimens were 3.234 and 3.224 g/cm^3, respectively. The measured values of fracture stress (σ_F), fracture toughness (K_{IC}), and elastic modulus (E) for Si_3N_4-A and Si_3N_4-B specimens are summarized in Table 1.

The fractographic observation of the fracture surfaces of the broken MOR bars indicated a mixed trans- and intergranular failure mode in both Si_3N_4-A and Si_3N_4-B specimens. The largest grains in Si_3N_4-A and Si_3N_4-B specimens were ≈7 and 3 μm in diameter, respectively. The failures were initiated primarily from surface flaws introduced during surface machining. The failure-initiating flaws were generally semielliptical and located in polycrystalline regions in both Si_3N_4-A and Si_3N_4-B specimens.

Figure 1 shows photomicrographs of a fracture surface of a hot-pressed Si_3N_4-A + 6% Y_2O_3 specimen; an outer fracture mirror and a failure causing flaw are indicated. According to the experimental observation of Mecholsky et al.,[8] the relationship of the outer fracture mirror radius (A_o) to the critical flaw size (C_c) is expressed by the equation

$$\frac{A_o}{C_c} = 13. \qquad (1)$$

The critical flaw size obtained form Eq. 1 by fracture mirror measurements agreed very well with the measured depth of the surface flaw. The size of the flaws in Si_3N_4-A and Si_3N_4-B specimens, as measured by fractography, generally ranged from 25 to 81 μm.

Table 2 shows the mechanical properties of Si_3N_4 specimens that contained Fe or Si inclusions. The data in Tables 1 and 2 show that inclusions have little effect on the fracture toughness (K_{IC}) of Si_3N_4 specimens. This is believed to be due to the fact that the indentation technique measures local fracture toughness and the toughness of the matrix was not affected in the region away from the Fe or Si inclusions. On the other hand, the strength (σ_F) of Si_3N_4 specimens that contained 0.5 and 5 wt.% Fe inclusions decreased by ≈15-40%, whereas that of specimens that contained 0.5 and 1 wt.% Si inclusions decreased by ≈39-50%. These reductions in strength are due to the formation of large critical flaws caused by the Fe and Si inclusions. Figure 2 shows typical critical flaws observed by fractography in Si_3N_4-Fe and Si_3N_4-Si specimens. These flaws were generally located within 150 μm of the tensile surface and included primarily Fe- and/or Si-rich inclusions and regions of degraded Si_3N_4 matrix attributable to interaction between molten metal (Fe or Si) and the matrix. The flaw size, which was defined as half the width (smallest dimension) of the internal flaws, ranged from ≈14 to 84 μm.

Correlation between Measured Critical Flaw Size and Mechanical Properties

To find a correlation between mechanical properties and critical flaw sizes measured by fractography, we calculated an effective critical flaw size by fracture mechanics analysis, based on measured mechanical properties. Subsequently, a comparison was made between the effective and measured critical flaw sizes to evaluate the above correlation. For semielliptical surface flaws, we calculated the effective critical flaw size C_e from the measured values of flexural strength σ_F and fracture toughness K_{IC} (Table 1) by using the relationship[11,12]

$$K_{IC} = 1.35\sigma_F\sqrt{C_e} \qquad (2)$$

Because the shape of the internal flaws was irregular, radii of hypothetical circular cracks that would fail at the same applied stress were calculated for the purpose of comparison with measured flaw sizes. We calculated the radius (a) of this effective critical circular flaw by using the relationship[13]

Table 1. Mechanical properties of hot-pressed Si_3N_4

Material	Fracture Stress σ_F (MPa)	Fracture Toughness K_{IC} (MPa$\sqrt{m}$)	Elastic Modulus E (GPa)
Si_3N_4-A + 6% Y_2O_3	839 ± 25	6.7 ± 0.09	296 ± 2
Si_3N_4-B + 6% Y_2O_3	1049 ± 118	6.4 ± 0.03	307 ± 6

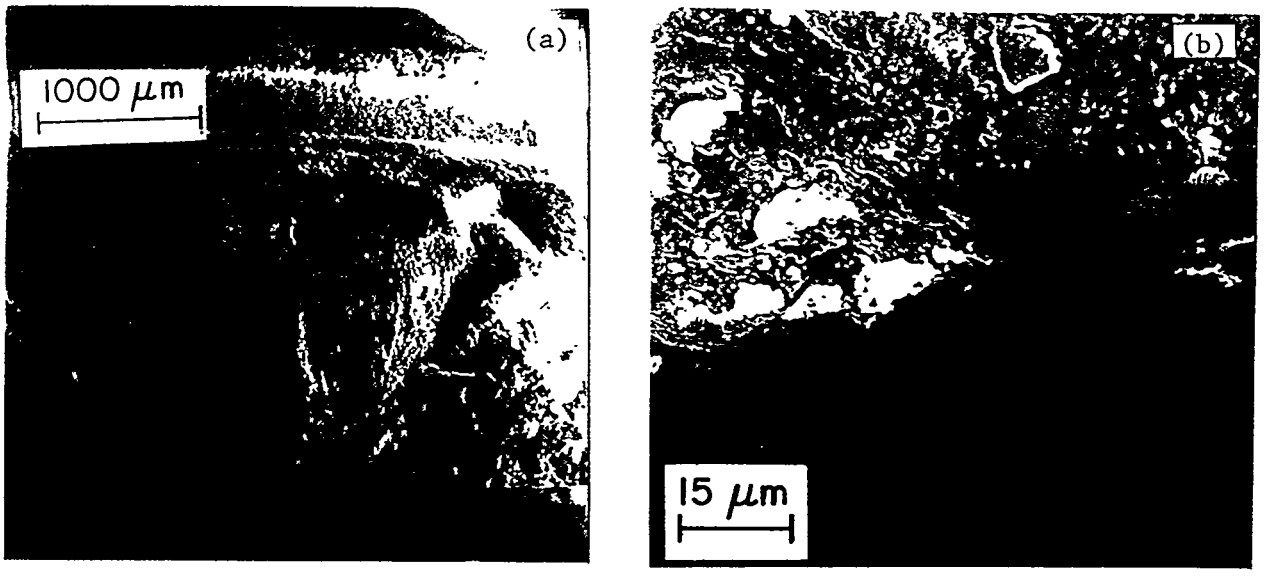

Fig. 1. Scanning electron micrographs of fracture surface of hot-pressed Si_3N_4-A + 6% Y_2O_3 specimen, showing (a) outer fracture mirror boundary (dashed line) and (b) typical surface flaw.

Table 2. Measured mechanical properties of hot-pressed Si_3N_4 + 6% Y_2O_3 with Fe or Si inclusions

Property	Si_3N_4-A		Si_3N_4-B	
	0.5 wt.% Fe	5 wt.% Fe	0.5 wt.% Si	1 wt.% Si
Flexural Strength, σ_F (MPa)	716 ± 84	507 ± 29	639 ± 110	521 ± 137
Fracture Toughness, K_{IC} (MPa$\sqrt{m}$)	6.53 ± 0.9[a]	6.53 ± 0.9	6.53 ± 0.9[a]	6.53 ± 0.9[a]
Elastic Modulus, E (GPa)	289 ± 2	303 ± 6	285 ± 1	-

[a]This value was assumed.

$$K_{IC}^2 = \left(\frac{4}{\pi}\right) a\sigma_a^2 , \qquad (3)$$

where σ_a is the applied stress at the critical internal flaw. The value of σ_a was calculated from the measured flexural strength σ_f, specimen thickness, and distance of the flaw from the tensile surface.

A comparison of the measured and calculated sizes of the critical surface flaws in Si_3N_4 + 6% Y_2O_3 specimens is shown in Table 3. The good agreement between the measured and calculated flaw sizes substantiates the validity of fracture mechanics calculations and fractographic observations. A similar comparison between the measured and calculated values of the critical flaw size for Si_3N_4 specimens with Fe or Si inclusions is shown in Figs. 3 and 4, respectively. Unlike the case of surface flaws, values of the critical internal flaw size that were calculated by fracture mechanics analysis were always greater than those that were measured. Similar observations were made by Baumgartner and Richerson[14] for inclusion-initiated fracture in hot-pressed Si_3N_4.

The tendency of fracture mechanics calculations to overestimate the size of critical internal flaws associated with these inclusions appears to be due partly to inaccurately assuming circular cracks and the corresponding K_{IC} for irregularly shaped internal flaws, and partly to the local degradation in fracture toughness (K_{IC}) at the matrix/inclusion interface. As suggested by Baumgartner and Richerson[14] and Singh,[15] the reduction in local K_{IC} is as much as 50% of the bulk value. Therefore, fracture mechanics predictions based on

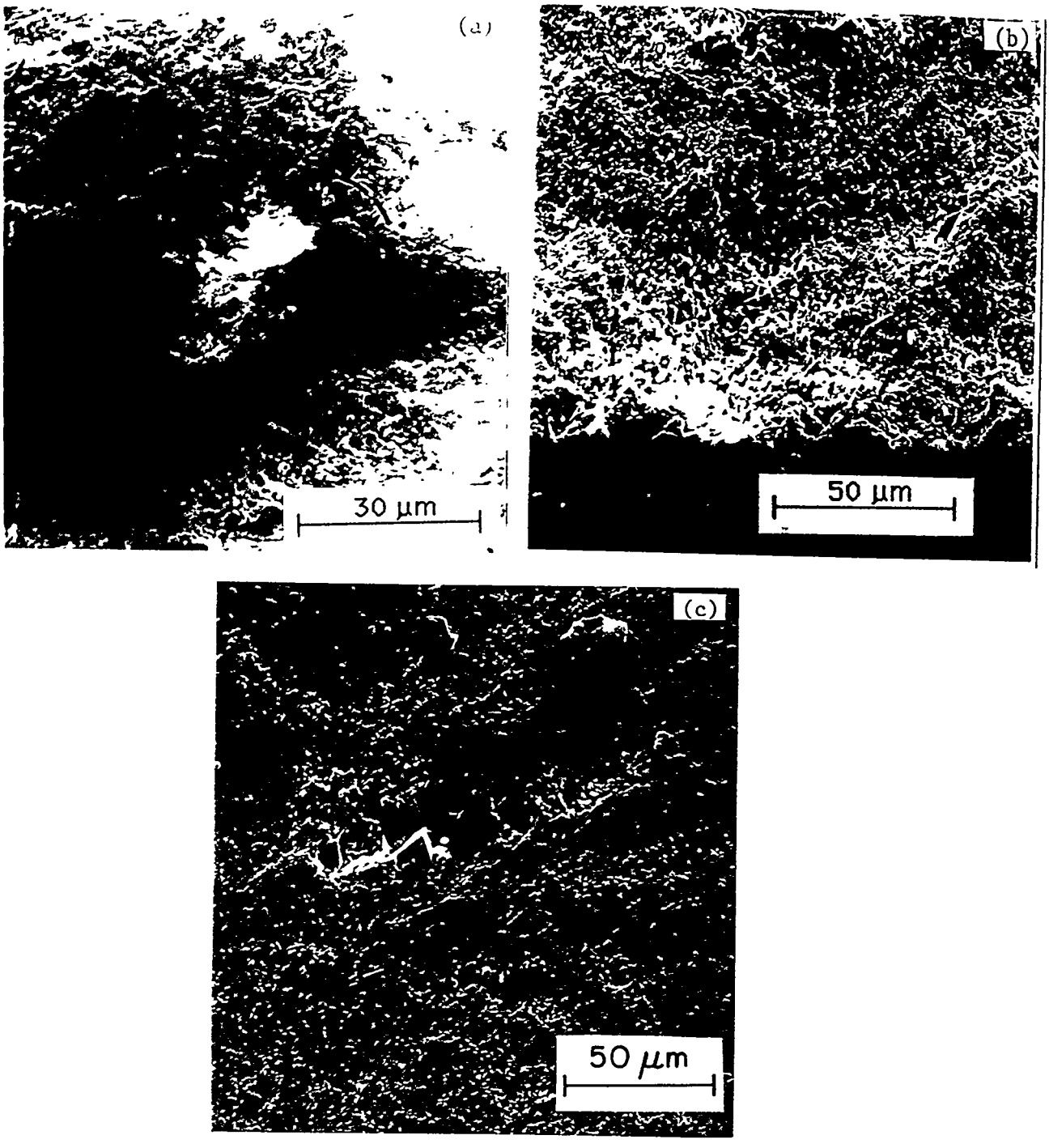

Fig. 2. Scanning electron photomicrographs of Si_3N_4-Fe and Si_3N_4-Si fracture surfaces showing typical internal flaws; (a) Fe-rich inclusion, (b) degraded Si_3N_4 matrix, and (c) Si-rich inclusion.

Table. 3. Calculated and measured values of critical flaw size

Material and Specimen No.	Critical Flaw Size (μm)	
	Measured	Calculated
Si_3N_4-A		
1	48	41
2	51	56
3	25	33
4	81	76
5	72	74
Si_3N_4-B		
1	30	26
2	33	21

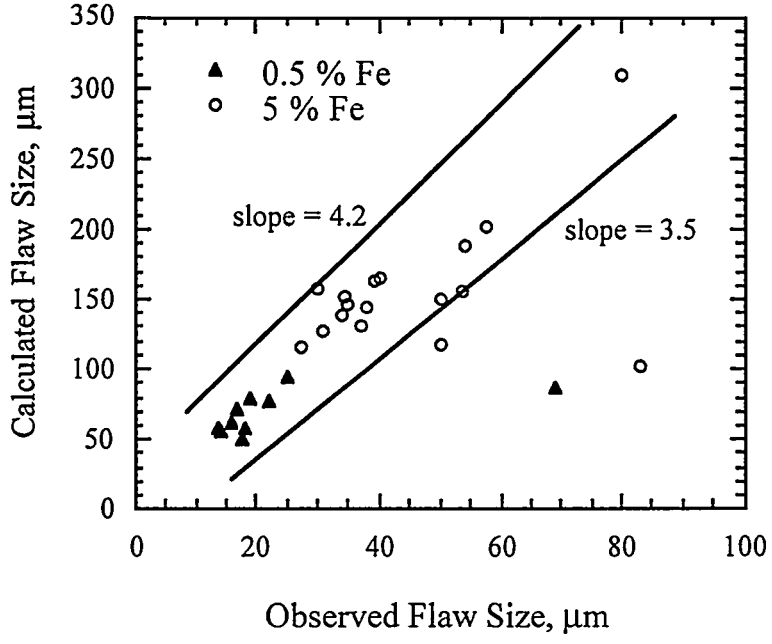

Fig. 3. Measured and calculated (effective) values of critical flaw size for Si_3N_4-Fe specimens.

a bulk K_{IC} value (which is higher than the local K_{IC}) overestimate the size of the critical internal flaw and may provide misleading conclusions unless caution is exercised.

The data shown in Figs. 3 and 4 also suggest the existence of a definite ratio K between calculated and measured flaw sizes. In general, the value of K ranges from 3.5 to 4.2 for Fe inclusions and 1.7 to 3.1 for Si inclusions. It is proposed that, for a given Fe inclusion size C_I (observed by fractography), an "effective flaw size" C_{eff} ($C_{eff} = KC_I$) can be obtained to predict the strength degradation due to inclusions more precisely. Determination of an effective flaw size will have important implications for prediction of failure in ceramics, based on the inclusion size indicated by microstructural observations and/or nondestructive evaluation data.

SUMMARY

The addition of 5 and 0.5 wt.% Fe inclusions of 88 to 250 μm size reduced the strength of Si_3N_4 specimens by ≈40 and 15%, respectively. The corresponding reduction in strength due to 1 and 0.5 wt.% Si of <149 μm size inclusions was 50 and 39%, respectively. This is believed to be due to formation of large flaws from the interaction between molten Fe (or Si) and the Si_3N_4 matrix.

Failure in Si_3N_4-Y_2O_3 specimens with Fe or Si inclusions occurred primarily from internal flaws located within ≈150 μm of the tensile surface. These flaws included Fe- and Si-rich inclusions and/or regions of the Si_3N_4 matrix that were degraded as a result of reaction between Si_3N_4 and molten Fe (or Si).

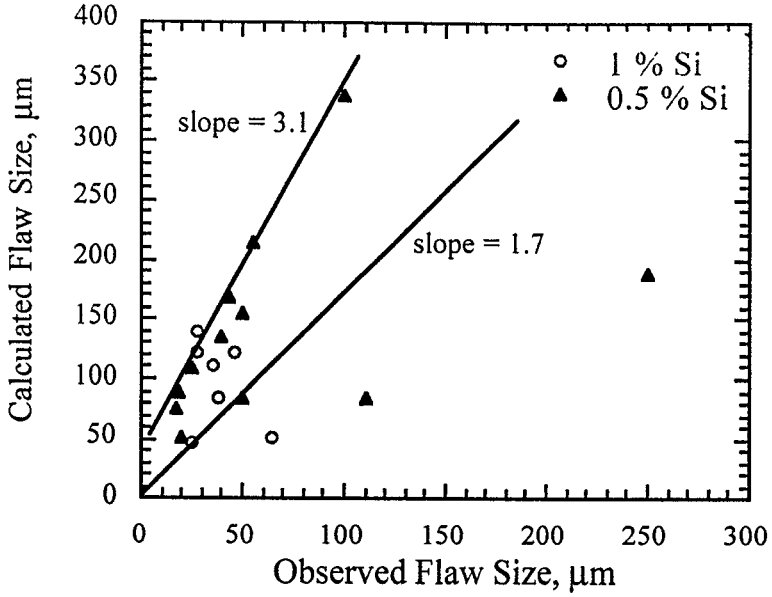

Fig. 4. Measured and calculated (effective) values of critical flaw xize for Si_3N_4-Si specimens.

For surface flaws, good agreement was observed between critical flaw sizes calculated by fracture mechanics analysis and those measured by fractography. On the other hand, for inclusion (Fe or Si)-induced internal flaws, the calculated flaw sizes were always larger than the measured sizes. This observation suggests local degradation in fracture toughness of the Si_3N_4 matrix. A ratio K (≈3.5-4.2 for Fe inclusions and 1.7-3.1 for Si inclusion) appears to exist between the calculated and measured critical internal flaw sizes. An effective flaw size C_{eff} can be determined from the observed flaw size C_I (i.e., $C_{eff} = KC_I$) to predict strength degradation due to inclusions.

ACKNOWLEDGMENTS

This research was supported by Office of Fossil Energy, U.S. Department of Energy, Advanced Research and Technology Development Fossil Energy Materials Program, under Contract W-31-109 Eng-38. Thanks are extended to R. B. Poeppel, Director of Argonne's Energy Technology Division, for frequent discussions and helpful comments.

REFERENCES

1. D. W. Richerson, Ceram. Bull. 64(2), 282-286 (1985).
2. D. C. Larsen and J. W. Adams, Air Force Wright Aeronautical Laboratories Report AFWAL-TR-83-4141, April 1984.
3. Katsutoshi Komeya, Am. Ceram. Soc. Bull., 63(9), 1158-1159 (1984).
4. Reliability of Ceramics for Heat Engine Applications, National Materials Advisory Board Report NMAB-357, 1980.
5. H. P. Kirchner, R. M. Gruver, and W. A. Sotter, Mater. Sci. Eng. 22(2), 147-156 (1976).
6. F. F. Lange, J. Am. Ceram. Soc. 66(6), 396-398 (1983).
7. J. W. Johnson and D. G. Holloway, Phil. Mag. 14, 731-743 (1966).
8. J. J. Mecholsky, Jr., S. W. Freiman, and R. W. Rice, J. Mater. Sci. 11, 1310-1319 (1976).
9. A. G. Evans, Fracture Mechanics Applied to Brittle Materials, S. W. Freiman, ed., ASTM STP 678 (ASTM, Philadelphia), pp. 112-135 (1979).

10. J. Krautkrämer and H. Krautkrämer, Ultrasonic Testing of Materials, Springer-Verlag, New York (1983).
11. A. S. Kobayashi, Proc. Second Int. Conf. on Mechanical Behavior of Materials, pp. 1073-1077 (August 1976).
12. C. A. Andersson and R. J. Bratton, Science of Ceramic Machining and Surface Finishing II, R. R. Hockey and R. W. Rice, eds., NBS Publication 562 (1979), pp. 463-476.
13. I. N. Sneddon, Proc. R. Soc. London, pp. 229-260, 187A (1946).
14. H. R. Baumgartner and D. W. Richerson, Fracture Mechanics of Ceramics, Vol. 1, R. C. Bradt, D. P. H. Hasselman and F. F. Lange, eds., Plenum Press, New York (1973), pp. 367-386.
15. J. P. Singh, Argonne National Laboratory Report ANL/FE-86-3, 1986.